7th ECCOMAS Thematic Conference on Smart Structures and Materials
SMART 2015
A.L. Araúo, C.A. Mota Soares, et al. (Editors)

THIN SHELLS WITH PIEZOELCTRIC TRANSDUCERS: THEORY, NUMERICAL MODELLING AND VERIFICATION

Michael Pieber*, **Michael Krommer**† & **Yury Vetyukov**†

* Institute of Mechatronics, University of Innsbruck
Technikerstrasse 13, A-6020 Innsbruck, Austria
michael.pieber@uibk.ac.at

†Institute of Mechanics and Mechatronics, Vienna University of Technology
Getreidemarkt 9, A-1060 Vienna, Austria
{michael.krommer,yury.vetyukov}@tuwien.ac.at

Keywords: Smart structures, Nonlinear Thin Piezoelectric Shells, Efficient Numerical Modelling.

Summary: *For the modelling of thin elastic shells with attached piezoelectric transducers, we consider a material surface with certain mechanical degrees of freedom in each point. Additionally, electrical unknowns are present within the domain, where the piezoelectric transducers are attached, such that the sensing and actuating behavior can be properly accounted for. The modelling is done in the geometrically nonlinear regime, but the electromechanically coupled constitutive relations are treated within the framework of Voigt's linear theory of piezoelectricity. Owing to the assumed thinness of the shell the influence of shear is neglected in the modeling. A Finite Element scheme for the solution of the resulting model is implemented and the solutions computed with the present theory are compared to results computed with the commercially available FE code Abaqus. Different examples are presented ranging from large deformations, to snap through instability and to a linear analysis. A very good agreement between the results is obtained, from which the accuracy of the thin shell formulation as a material surface is concluded. Next, an existing physical shell is modeled within the linearized version of the present theory and the computational results are compared to measurement results from the physical experiment. The agreement is reasonably good; natural frequencies as well as eigenmodes are considered for the comparison. Concerning the eigenmodes the* MAC *criterion is used. Finally, the resulting linear time invariant dynamical system for the simulation of the physical shell is imported into Mathematica and different strategies for passive and active control are tested and compared to each other. Concerning passive control methods classical single mode shunt-damping using an optimized RL-network is studied.*

1. INTRODUCTION

Many practical problems, like active or passive vibration control and the study of buckling and post-buckling of thin piezoelectric shells require the proper electromechanically coupled

modeling of the shell; both, in the linear and the nonlinear regime. In particular, the effect of electromechanical coupling must be properly accounted for on the level of a theory of structural mechanics for thin shells.

Different approaches to reduce the three dimensional equations to the structural level range from equivalent single-layer theories (Krommer[1] or Batra and Vidoli[2]), to layer-wise formulations and to hybrid or mixed formulations, see Carrera and Boscolo[3] for a review in the case of piezoelectric plates. In these theories a-priori assumptions concerning the distribution of the displacement vector and the electric potential through the thickness of a thin structure are imposed and the resulting governing equations are derived using a weak form of the three dimensional equations. In the present paper a nonlinear theory for thin piezoelectric shells is presented, which considers the shell as a material surface with certain mechanical degrees of freedom in each point. Additionally, electrical unknowns are present within the domain, where the piezoelectric transducers are attached, such that the sensing and actuating behavior can be properly accounted for. The modelling is done in the geometrically nonlinear regime, but the electromechanically coupled constitutive relations are treated within the framework of Voigt's linear theory of piezoelectricity. Owing to the assumed thinness of the shell the influence of shear is neglected in the modeling. The present formulation for the shell represents an extension of a linear formulation derived in Krommer [1] for thin plates, which has been recently proven to be asymptotically exact, see Vetyukov et.al. [4]

2. GEOMETRICALLY NONLINEAR MODELING OF THIN PIEZOELECTRIC SHELLS

In the present paper a theory is developed, for which a thin shell is considered as a material surface with mechanical and electrical degrees of freedom.

2.1 Differential geometry of a surface

As a starting point, we introduce some notions from differential geometry of a surface. We consider an undeformed reference configuration of the shell, in which a material point of the reference surface has the position vector $\mathbf{R}(q^\alpha)$; q^1 and q^2 are the curvlinear Lagrangean coordinates of the reference surface. We denote the derivatives of an entity with respect to these coordinates as $\partial/\partial q^\alpha \equiv \partial_\alpha$. The base vectors $\mathbf{R}_\alpha$ in the tangential plane and the unit normal vector $\mathbf{N}$ are

$$\mathbf{R}_\alpha = \partial\mathbf{R}/\partial q^\alpha\,,\ \mathbf{N} = \mathbf{R}_1 \times \mathbf{R}_2 / \left\|\mathbf{R}_1 \times \mathbf{R}_2\right\|. \tag{1}$$

Fig. 1 shows the basic concepts we just introduced. We are now in the position to proceed further. First, we define the 2D differential operator with respect to the reference configuration as

$$\overset{\circ}{\nabla} = \mathbf{R}^\alpha \partial_\alpha, \tag{2}$$

and compute the first metric tensor $\mathbf{A}$ and the second metric tensor $\mathbf{B}$ from

$$\mathbf{A} = \overset{\circ}{\nabla}\mathbf{R} = \mathbf{I} - \mathbf{N}\mathbf{N}\,,\ \mathbf{B} = -\overset{\circ}{\nabla}\mathbf{N}. \tag{3}$$

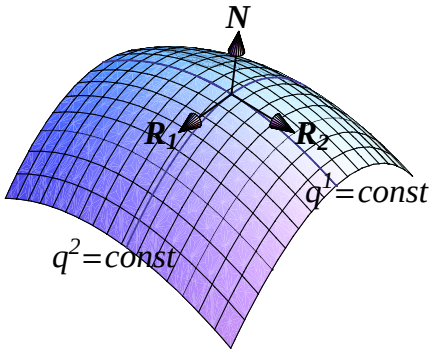

Figure 1. Shell as a material surface

Finally, the area element in the reference configuration is $d\overset{\circ}{\Omega} = \sqrt{A}dq^1dq^2$, in which $A = \|\mathbf{R}_1 \times \mathbf{R}_2\|^2$.

Next, we consider the deformed configuration, in which lower case letters are used. The position vector is $\mathbf{r} = \mathbf{r}(q^\alpha)$, and we can introduce the corresponding entities in the actual configuration $\mathbf{r}_\alpha$, $\mathbf{n}$, ∇, $\mathbf{a}$, $\mathbf{b}$ and $d\Omega$, which are defined indentical to the ones in the reference configuration, besides the use of the differential operator ∇ with respect to the actual configuration. The two configurations are linked to each other by means of the deformation gradient tensor

$$\mathbf{F} = \left(\overset{\circ}{\nabla}\mathbf{r}\right)^T = \mathbf{r}_\alpha\mathbf{R}^\alpha. \tag{4}$$

Note that the inverse of this tensor does not exist; nonetheless, we will also use the notion $\mathbf{F}^{-1}$ for the pseudo inverse of the deformation gradient tensor. The latter is defined as $\mathbf{F}^{-1}\cdot\mathbf{F} = \mathbf{A}$ and $\mathbf{F}\cdot\mathbf{F}^{-1} = \mathbf{a}$. The relation between the area elements in the two configurations is $d\Omega = Jd\overset{\circ}{\Omega}$, with $J = \sqrt{a/A}$.

2.2 Basic shell equations

Now, consider a shell as a two-dimensional continuum of "needles" with five degrees of freedom: three translations $\delta\mathbf{r}$ and two rotations $\delta\mathbf{n}$; the variation of the unit normal vector lies in the tangential plane. This resembles the notion of a single director attached to each particle of the shell, introduced by Naghdi [5]. Then, the principle of virtual work work reads

$$\int_\Omega \left(\mathbf{q}\cdot\delta\mathbf{r} + \mathbf{m}\times\mathbf{n}\cdot\delta\mathbf{n} + J^{-1}\delta A^i\right)d\Omega + \int_{\partial\Omega}\left(\mathbf{P}\cdot\delta\mathbf{r} + \mathbf{M}\times\mathbf{n}\cdot\delta\mathbf{n}\right)dl = 0, \tag{5}$$

in which $\mathbf{q}$ and $\mathbf{m}$ are distributed external forces and moments per unit area in the deformed configuration and $\mathbf{P}$ and $\mathbf{M}$ are distributed boundary forces and moments per unit length in the deformed configuration; for details see Eliseev and Vetyukov [6]. δA^i is the virtual work of the internal forces per unit area in the reference configuration. We introduce geometrically

nonlinear strain tensors according to the change of the metric of the surface as

$$\begin{aligned}\mathbf{C} &= \frac{1}{2}\left(\mathbf{F}^T\cdot\mathbf{F}-\mathbf{a}\right) = C_{\alpha\beta}\mathbf{R}^\alpha\mathbf{R}^\beta\,,\ C_{\alpha\beta}=\frac{1}{2}\left(A_{\alpha\beta}-a_{\alpha\beta}\right)\\ \mathbf{K} &= \mathbf{F}^T\cdot\mathbf{B}\cdot\mathbf{F}-\mathbf{b} = K_{\alpha\beta}\mathbf{R}^\alpha\mathbf{R}^\beta\,,\ K_{\alpha\beta}=B_{\alpha\beta}-b_{\alpha\beta}.\end{aligned}\tag{6}$$

Both, $\mathbf{C}$ and $\mathbf{K}$ vanish in the reference configuration. Moreover, they remain constant, if and only if the shell undergoes a rigid body motion and the virtual work of the internal forces does not change; then,

$$\delta\mathbf{C}=\mathbf{0}\,,\quad \delta\mathbf{K}=\mathbf{0}\quad\rightarrow\quad \delta A^i=0\tag{7}$$

must hold for a classical non-shearable shell. This means the orthogonality of $\mathbf{n}$ and $\mathbf{r}_\alpha$; therefore,

$$\delta\left(\mathbf{r}_\alpha\cdot\mathbf{n}\right)=0\quad\rightarrow\quad \nabla\delta\mathbf{r}\cdot\mathbf{n}+\delta\mathbf{n}=0\tag{8}$$

must hold as well. Now, we consider the principle of virtual work under the above constraints, for which we introduce Lagange multipliers $\boldsymbol{\tau}$, $\boldsymbol{\mu}$ and $\mathbf{Q}$, such that the term $J^{-1}\delta A^i$ can be formally replaced by

$$J^{-1}\delta A^i\rightarrow -\mathbf{F}^{-1}\cdot\boldsymbol{\tau}\cdot\mathbf{F}^{-T}\cdot\cdot\,\delta\mathbf{C}-\mathbf{F}^{-1}\cdot\boldsymbol{\mu}\cdot\mathbf{F}^{-T}\cdot\cdot\,\delta\mathbf{K}+\mathbf{Q}\cdot\left(\delta\mathbf{n}+\nabla\delta\mathbf{r}\cdot\mathbf{n}\right)\tag{9}$$

in the principle of virtual work. The equilibrium conditions are now derived from the principle of virtual work as

$$\nabla\cdot\mathbf{T}+\mathbf{q}=\mathbf{0}\,,\quad \mathbf{Q}+\nabla\cdot\boldsymbol{\mu}\cdot\mathbf{a}-\mathbf{m}\times\mathbf{n}=\mathbf{0},\tag{10}$$

in which $\mathbf{T}=\boldsymbol{\tau}+\boldsymbol{\mu}\cdot\mathbf{b}+\mathbf{Q}\mathbf{n}$. $\boldsymbol{\tau}$ and $\boldsymbol{\mu}$ are Cauchy-type stress tensors and $\mathbf{Q}$ is the transverse shear force vector, which can only be computed from the equilibrium conditions, but not from a constitutive relation. The equilibrium conditions refer to the deformed configuration. One could derive a corresponding formulation refering to the reference configuration involving Piola-type stress tensors. For details, also concerning boundary conditions, we refer to Vetyukov [7].

The present formulation must be completed by constitutive relations. For that sake we introduce a specific 2D enthalpy as

$$\eta_0 H_2=\frac{1}{2}\mathbf{C}\cdot\cdot\,\mathbb{A}\cdot\cdot\,\mathbf{C}+\mathbf{C}\cdot\cdot\,\mathbb{B}\cdot\cdot\,\mathbf{K}+\frac{1}{2}\mathbf{K}\cdot\cdot\,\mathbb{D}\cdot\cdot\,\mathbf{K}-V_i(\mathbf{p}_i\cdot\cdot\,\mathbf{C}+\mathbf{s}_i\cdot\cdot\,\mathbf{K})-\frac{1}{2}c_iV_i^2.\tag{11}$$

η_0 is the mass per unit area in the undeformed configuration. $\mathbb{A}$, $\mathbb{B}$ and $\mathbb{D}$ are stifness tensors, $\mathbf{p}_i$ and $\mathbf{s}_i$ are tensors of piezoelectric coefficients and c_i are specific capacities. All these entities are taken from a linear piezoelectric plate theory, see e.g. Krommer [1] or Vetyukov et.al. [4] for details concerning their definition. V_i are the electric voltages. E.g. in a layered shell more than one layer may exhibit piezoelectric material parameter, such that one voltage per piezoelectric layer would enter the formulation. Now we can compute the Cauchy-type stress tensors used in the equilibrium conditions from the derivatives of the specific enthalpy as

$$\boldsymbol{\tau}=\eta_0J^{-1}\mathbf{F}\cdot\frac{\partial H_2}{\partial\mathbf{C}}\cdot\mathbf{F}^T\,,\quad \boldsymbol{\mu}=\eta_0J^{-1}\mathbf{F}\cdot\frac{\partial H_2}{\partial\mathbf{K}}\cdot\mathbf{F}^T\,,\quad q_i=-\eta_0\frac{\partial H_2}{\partial V_i}.\tag{12}$$

Here, q_i is an electric charge per unit area in the undeformed configuration. The latter can be integrated over the shell domain in case a piezoelectric layer is considered or over the doamin of a piezoelectric patch $\overset{\circ}{\Omega}_i$; in any case the voltage V_i is constant with respect to these domains, as they are in general electroded. Hence, we have

$$\Sigma_i = \int\limits_{\overset{\circ}{\Omega}_i} q_i d\,\overset{\circ}{\Omega}. \tag{13}$$

With the second Piola-Kirchhoff stress tensors $\overset{\circ}{\boldsymbol{\tau}} = J\mathbf{F}^{-1}\cdot\boldsymbol{\tau}\cdot\mathbf{F}^{-T}$ and $\overset{\circ}{\boldsymbol{\mu}} = J\mathbf{F}^{-1}\cdot\boldsymbol{\mu}\cdot\mathbf{F}^{-T}$ the constitutive relations are

$$\begin{aligned}
\overset{\circ}{\boldsymbol{\tau}} &= \eta_0\frac{\partial H_2}{\partial\mathbf{C}} = \mathbb{A}\cdot\cdot\,\mathbf{C} + \mathbb{B}\cdot\cdot\,\mathbf{K} - \mathbf{p}_i V_i,\\
\overset{\circ}{\boldsymbol{\mu}} &= \eta_0\frac{\partial H_2}{\partial\mathbf{K}} = \mathbb{B}\cdot\cdot\,\mathbf{C} + \mathbb{D}\cdot\cdot\,\mathbf{K} - \mathbf{s}_i V_i,\\
\Sigma_i &= -\int\limits_{\overset{\circ}{\Omega}_i}\eta_0\frac{\partial H_2}{\partial V_i}d\,\overset{\circ}{\Omega} = C_i V_i + \int\limits_{\overset{\circ}{\Omega}_i}(\mathbf{p}_i\cdot\cdot\,\mathbf{C} + \mathbf{s}_i\cdot\cdot\,\mathbf{K})d\,\overset{\circ}{\Omega},
\end{aligned} \tag{14}$$

in which C_i is the total capacity of either the piezoelectric layer or the piezoelectric patch. The last relation is a transducer relation, which relates the total charge not only to the voltage via the capacity, but also to the strain tensors via the direct piezoelectric effect. As we have already mentioned, we are not interested in formulating the equilibrium conditions and the boundary conditions in terms of the Piola-Kirchhoff stress tensors; rather, we conclude this section with a variational statement of the problem.

2.3 Variational formulation

We complete the development of the shell theory by formulating an extension of the principle of virtual work with respect to electromechanical coupling. For the virtual work of the external loadings (forces, moments and electrical charges) we have

$$\delta A^e = \int\limits_{\overset{\circ}{\Omega}}\overset{\circ}{\mathbf{q}}\cdot\delta\mathbf{r}d\overset{\circ}{\Omega} + \tilde{\Sigma}_i\delta V_i. \tag{15}$$

For the sake of simplicity, we only account for distributed forces per unit area in the undeformed configuration $\overset{\circ}{\mathbf{q}} = J\mathbf{q}$, but not for distributed moments or any forces and moments applied at the boundary. $\tilde{\Sigma}_i$ are the applied charges at the electrodes. The virtual work of the internal loadings is

$$\delta A^i = -\int\limits_{\overset{\circ}{\Omega}}\left(\overset{\circ}{\boldsymbol{\tau}}\cdot\cdot\;\delta\mathbf{C} + \overset{\circ}{\boldsymbol{\mu}}\cdot\cdot\;\delta\mathbf{K}\right)d\overset{\circ}{\Omega} - \Sigma_i\delta V_i = -\delta\int\limits_{\overset{\circ}{\Omega}}\eta_0 H_2(\mathbf{C},\mathbf{K},V_i)d\overset{\circ}{\Omega}, \tag{16}$$

such that the principle of virtual work reads

$$\int\limits_{\overset{\circ}{\Omega}}\left(\overset{\circ}{\mathbf{q}}\cdot\delta\mathbf{r} - \overset{\circ}{\boldsymbol{\tau}}\cdot\cdot\;\delta\mathbf{C} - \overset{\circ}{\boldsymbol{\mu}}\cdot\cdot\;\delta\mathbf{K}\right)d\overset{\circ}{\Omega} + \left(\tilde{\Sigma}_i - \Sigma_i\right)\delta V_i = 0. \tag{17}$$

Using the enthalpy and assuming all external loadings to be conservative $\delta A^e = -\delta U^e$, then the principle of virtual work can be rewritten as

$$\delta A^i + \delta A^e = -\delta \left(U^{H_2} + U^e \right) = -\delta U^\Sigma = 0, \tag{18}$$

with

$$U^{H_2} = \int_{\overset{\circ}{\Omega}} \eta_0 H_2(\mathbf{C}, \mathbf{K}, V_i) d\overset{\circ}{\Omega}, \tag{19}$$

from which we conclude that the total energy functional $U^\Sigma = U^{H_2} + U^e$ must have a stationary value for an equilibrium.

2.4 Finite Element modeling

For the Finite Element implementation we use elements with 4 nodes. Each node has 12 mechanical degrees of freedom, which are the position vector $\mathbf{r}$, the base vectors in the deformed configuration $\mathbf{r}_\alpha$ and the vectors of mixed derivatives of the position vector $\mathbf{r}_{\alpha\beta}$, see Vetyukov [8]. The domain of an element is $\Omega_{el} = q^1 \times q^2$, in which the local coordinates have the range $[-1, 1]$. The position vector within the j-th element is approximated as

$$\mathbf{r}^j(q^1, q^2) = \sum_{i=1}^{n} S^{i,1}(q^1, q^2)\mathbf{r}^j + S^{i,2}(q^1, q^2)\mathbf{r}_1^j + S^{i,3}(q^1, q^2)\mathbf{r}_2^j + S^{i,4}(q^1, q^2)\mathbf{r}_{12}^j. \tag{20}$$

The four bi-cubic shape functions are shwon in Fig. 2. The element degrees of freedom are borrowed from the global vector of degrees of freedom $\mathbf{U}$, which contains all mechanical degrees of freedom. The voltages at the electroded layers or patches are collected in the vector $\mathbf{V}$. For

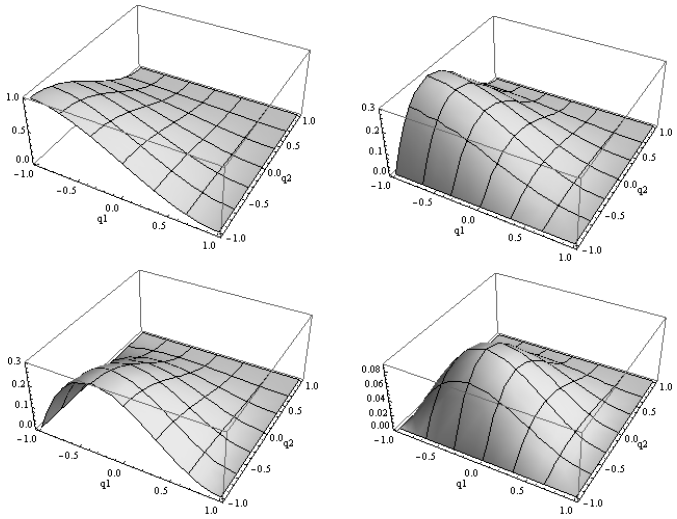

Figure 2. Shape functions

all elements with electrical degrees of freedom these unknowns are borrowed from $\mathbf{V}$, which

ensures the equipotential area condition at the electrodes. As the electric potentials are element wise constant, no approximation is needed for the voltages within the element. Finally, we seek for an extremum of the total energy functional,

$$U^{\Sigma} = \left(U^{H_2} + U^{e}\right) \quad \rightarrow \quad Extremum, \tag{21}$$

provided the problem is conservative. This will be the case in all examples.

3. VERIFICATION

In order to verify our theory and its FE implementation we compare the results of our simulations to the results of computations with the commercial FE code ABAQUS in this section. In particular, we consider plates in the geometrically linear regime and shells in the geometrically nonlinear regime. As we will be discussing below, an electromechanically coupled shell formulation is unavailable in ABAQUS, such that one needs to involve three-dimensional finite elements for the present kind of problems.

3.1 Linear plates

Within this subsection, we restrict ourselves to plates in the geometrically linear regime. The governing equations are obtained from our FE implementation using an initially flat reference configuration and linearizing the system of algebraic equations for the deformation in the vicinity of the reference configuration. Moreover, inertia is included in the formulation in terms of a kinetic energy, with

$$T = \frac{1}{2}\int_{\mathring{\Omega}} \eta_0 \dot{\mathbf{r}} \cdot \dot{\mathbf{r}} d\mathring{\Omega}, \tag{22}$$

from which a mass matrix can be computed in a straight forward manner. The result is a system of second order linear ordinary differential equations with constant coefficients,

$$\begin{bmatrix} \mathbf{M} & \mathbf{0} \\ \mathbf{0} & \mathbf{0} \end{bmatrix} \begin{bmatrix} \ddot{\mathbf{U}} \\ \ddot{\mathbf{V}} \end{bmatrix} + \begin{bmatrix} \mathbf{K}_{uu} & \mathbf{K}_{uv} \\ \mathbf{K}_{uv}^T & \mathbf{K}_{vv} \end{bmatrix} \begin{bmatrix} \mathbf{U} \\ \mathbf{V} \end{bmatrix} = \begin{bmatrix} \mathbf{F} \\ \mathbf{Q} \end{bmatrix}, \tag{23}$$

in which $\mathbf{U}$ is the vector of mechanical nodal degrees of freedom, $\mathbf{V}$ the vector of voltages, $\mathbf{F}$ the vector of force loadings and $\mathbf{Q}$ the vector of electrical charges. We consider three cases in the following:

1. **The voltage is known:** In this case $\mathbf{V}$ can be elliminated and an effective load vector $\mathbf{F}_{eff} = \mathbf{F} - \mathbf{K}_{uv}\mathbf{V}$ replaces the original load vector in the equations, which reduce to

   $$\mathbf{M}\ddot{\mathbf{U}} + \mathbf{K}_{uu}\mathbf{U} = \mathbf{F}_{eff}. \tag{24}$$

   In a post computation the accumulated total charge can be found from

   $$\mathbf{Q} = \mathbf{K}_{uv}^T\mathbf{U} + \mathbf{K}_{vv}\mathbf{V}. \tag{25}$$

   This case includes also the case of a short-circuit $\mathbf{V} = \mathbf{0}$, in which the vector of charges can be measured, $\mathbf{y} = \mathbf{Q} = \mathbf{K}_{uv}^T\mathbf{U}$.

2. **The charge is known:** Then the voltage $\mathbf{V}$ is an unknown, but we can reduce the system of equations using
$$\mathbf{V} = \mathbf{K}_{vv}^{-1}\mathbf{Q} - \mathbf{K}_{vv}^{-1}\mathbf{K}_{uv}^{T}\mathbf{U}. \tag{26}$$
This results into
$$\mathbf{M}\ddot{\mathbf{U}} + \left(\mathbf{K}_{uu} - \mathbf{K}_{uv}\mathbf{K}_{vv}^{-1}\mathbf{K}_{uv}^{T}\right)\mathbf{U} = \mathbf{F}_{eff}, \tag{27}$$
with the effective force vector $\mathbf{F}_{eff} = \mathbf{F} - \mathbf{K}_{uv}\mathbf{K}_{vv}^{-1}\mathbf{Q}$. This case also includes the case of an open-circuit $\mathbf{Q} = \mathbf{0}$, in which the vector of voltages can be measured, $\mathbf{y} = \mathbf{V} = -\mathbf{K}_{vv}^{-1}\mathbf{K}_{uv}^{T}\mathbf{U}$.

3. **Neither the charge nor the voltage are known:** In this case the transducer must be connected to an electrical network or to a control system, such that an additional relation between the charge and the voltage can be specified to complete the problem. An example would be a passive network with a series connection of a resistor and an inductance; in this latter case, which is also denoted as *passive shunt damping* this relation is an ordinary differential equation,
$$\mathbf{V} = \mathbf{R}\dot{\mathbf{Q}} + \mathbf{L}\ddot{\mathbf{Q}}. \tag{28}$$
The matrices $\mathbf{R}$ and $\mathbf{L}$ are diagonal. The reformulated problem reads
$$\begin{bmatrix} \mathbf{M} & \mathbf{K}_{uv}\mathbf{L} \\ \mathbf{0} & \mathbf{K}_{vv}\mathbf{L} \end{bmatrix}\begin{bmatrix} \ddot{\mathbf{U}} \\ \ddot{\mathbf{Q}} \end{bmatrix} + \begin{bmatrix} \mathbf{0} & \mathbf{K}_{uv}\mathbf{R} \\ \mathbf{0} & \mathbf{K}_{vv}\mathbf{R} \end{bmatrix}\begin{bmatrix} \dot{\mathbf{U}} \\ \dot{\mathbf{Q}} \end{bmatrix} + \begin{bmatrix} \mathbf{K}_{uu} & \mathbf{0} \\ \mathbf{K}_{uv}^{T} & -\mathbf{I} \end{bmatrix}\begin{bmatrix} \mathbf{U} \\ \mathbf{Q} \end{bmatrix} = \begin{bmatrix} \mathbf{F} \\ \mathbf{0} \end{bmatrix}, \tag{29}$$
in which the vector of charges is unknown. In any case other control laws can be implemented here. We also note that this third case includes both, the short-circuit case and the open-circuit case. For the open-circuit case the impedance tends to infinity, for the short-circuit case the admittance tends to infinity.

In case more than one piezoelectric layer or patch are embedded or attached to the structure, combinations of the above cases are possible; the resulting equations can be easily obtained from the three individual formulations above.

Next, we will compare the results obtained from our shell FE implementation, which we denote as FE2 with results computed with ABAQUS. Here, we use 3D coupled elements in ABAQUS first and secondly, we study the implementation with structural shell elements coupled to electromechanical 3D elements to model the piezoelectric parts of the structure in ABAQUS.

3.1.1 Comparison to 3D piezoelectric Finite Elements

As a first example we study a square plate with the side length $a = 0.5$m and a total thickness $h = 0.003$m. The plate is made of three layers with identical thickness; the top layer and the bottom layer are made of the piezoelectric material PZT-5A and the center layer is made of Aluminum. PZT-5A is transversally isotropic and Aluminum is isotropic; hence, the sufficient material parameters (SI units are understood) are
$$E = 7.0 \times 10^{10}\,,\ \mu = 0.33\,,\ \rho = 2660 \tag{30}$$

for Aluminum and

$$C_{11} = 12.1 \times 10^{10}\,,\ C_{33} = 11.1 \times 10^{10}\,,\ C_{12} = 7.54 \times 10^{10},$$
$$C_{13} = 7.52 \times 10^{10}\,,\ C_{44} = 2.11 \times 10^{10}\,,\ \rho = 7500,$$
$$\epsilon_z = 1700\epsilon_0\,,\ e_{31} = -5.4\,,\ e_{33} = 15.8 \tag{31}$$

for PZT-5A. In particular, we study two cases: (1) all edges are clamped and (2) one edge is clamped and the other three edges are free. The results computed with FE2 using 400 (20×20) elements are compared to results computed with ABAQUS. For the 3D formulation we used 10.000 *C3D20E* elements for the piezoelectric layers and 20.000 *C3D20* elements for the Aluminum layer. The first 6 natural frequencies for the two models are presented in Tab. 1. Allthough the relative error in case of the cantilevered plate goes up to 3% the correspondance

Clamped	1	2	3	4	5	6
ABAQUS f/Hz	177.64	362.43	362.43	532.41	650.56	653.62
FE2 f/Hz	178.13	363.32	363.32	535.70	651.39	651.39
relative error e/%	0.28	0.25	0.25	0.62	0.13	0.13

Cantilvered	1	2	3	4	5	6
ABAQUS f/Hz	17.720	39.680	103.57	135.94	146.99	257.66
FE2 f/Hz	17.710	40.780	103.73	137.07	149.63	263.27
relative error e/%	-0.05	2.76	0.16	0.83	1.80	2.18

Table 1. Natural frequencies of the square plate

is in general very good considering the fact that we only use 400 elements in our code instead of 40.000 elements in ABAQUS. The high number of elements in ABAQUS may seem to be excessive, but it is actually neccesary in the following static computations. Besides the natural frequencies the eigenmodes are of interest for us too. We compute them with both, FE2 and ABAQUS, and present the *MAC* (Modal Assurance Criterium) between the two. The result is graphically represented in Fig. 3. Again we notice a good modal correlation between FE2 and ABAQUS. Finally, we consdier the problem of static equilibrium, in which an electric voltage is applied at the electrodes of the top layer and the bottom layer is used as a sensor to measure the resulting voltage from the deformation. The sensor voltage V_{bot}, the mid point deflection w and the accumalted charge at the actuator Σ_{top} are compared in Tab. 2 for an applied voltage $V_{top} = -1$V. For the case of the clamped plate, the present theory does not result into any mid point deflection nor a sensor voltage; the reason is that the clamping prevents the plate from any deformation and, hence, the voltage must be zero as well. In the ABAQUS results, both the mid point deflection and the voltage are very small, but not zero. This can be explained by the fact that in the 3D solution the actuation, which is applied non symmetrically with respect to the middle surface, also results into a change in the thickness of the upper piezoelectric layer, which is constraint by the clamping. Therefore, a small deflection occurs and a voltage can be

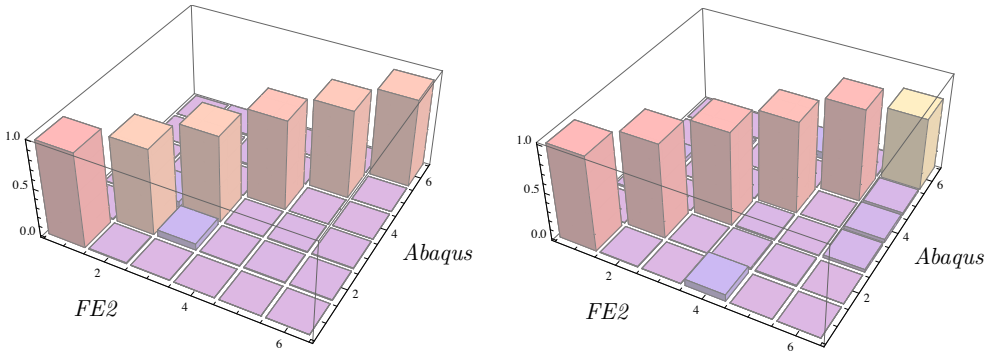

Figure 3. MAC for the rectangular plate with different boundary conditions: Clamped (left) and cantilevered (right)

Clamped	w/m	V_{bot}/V	Σ_{top}/C
ABAQUS	3.44×10^{-9}	-1.88×10^{-5}	4.32×10^{-6}
FE2	1.52×10^{-20}	-1.01×10^{-13}	4.33×10^{-6}
relative error e/%	-	-	-

Cantileverd	w/m	V_{bot}/V	Σ_{top}/C
ABAQUS	-1.20×10^{-5}	-1.82×10^{-2}	5.26×10^{-6}
FE2	-1.20×10^{-5}	-1.80×10^{-2}	5.26×10^{-6}
relative error e/%	0.27	-0.81	-0.01

Table 2. Comparison for the static transducer behavior

measured. The results for the accumulated charge at the actuator electrodes are very close as it is dominated by the capacitive behavior of the layer. No error is presented, because the results cannot be compared due to the fact the present theory prevents any thickness deformation. A different result is found for the cantilevered plate, where the response is dominated by bending. Here, the results coincide very well and the relative errors are very small. From the results we have presented in this section, we conclude that the present electromechanically coupled theory is capable of providing an accurate response and it is well suited for dynamic simulations including pasive and active control. In contrast, the 3D model in ABAQUS has a very high number of degrees of freedom and is therefore not suited for control applications, with the neccesity of a simple model with sufficient accuracy. This neccesity is met by the present formulation. Nonetheless, we must also mention the fact that one can also use structural shell elements in ABAQUS; yet, these elements have no electrical degrees of freedom. Therefore, they must be coupled with 3D piezoelectric elements.

3.1.2 Comparison to structural elements coupled with 3D piezoelectric Finite Elements

Here, we consider the problem shown in Fig. 4. The plate is rectangular and it has two attached piezoelectric patches with different dimensions, but identical position; one at the upper

side and one at the lower side. The material of the substrate plate is Aluminum and the piezoelectric patches are made of PZT-5A; the material parameters are the ones used in the previous example. The boundary is clamped. The geometry parameters are given in Tab. 3. The plate

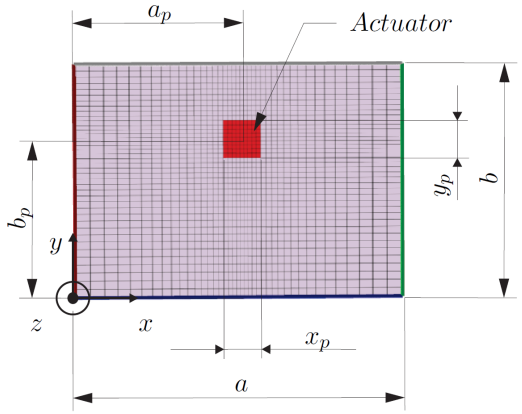

Figure 4. Sketch of the plate with piezoelectric patches

Length of plate a	0.87m
Width of plate b	0.62m
Thickness of substrate plate h	0.0008m
Distance to actuator and sensor a_p	0.444m
Distance to actuator and sensor b_p	0.420m
Length of actuator x_a	0.102m
Width of actuator y_a	0.102m
Height of actuator h_a	0.0002m
Length of sensor x_s	0.01m
Width of sensor y_s	0.01m
Height of sensor h_s	0.0002m

Table 3. Geometry parameters of the plate

is modelled in FE2 with a total of 40×40 elements, the domain of the actuator with 9×9 elements and the domain of the smaller sensor with 1 element. In ABAQUS two models are created. First, both the substrate plate and the actuator and sensor are modelled with 3D elements; for the plate *C3D20* elements are used, for the actuator and the sensor *C3D20E* elements are used. In total 56336 elements are used. We denote this type of modelling as ABAQUS VOLUME. Secondly, the substrate plate is modelled with 11672 structural shell elements of type *S85R*, the actuator with 2025 *C3D20E* elements and the sensor with 25 *C3D20E* elements. This type of modelling is denoted as ABAQUS SHELL. The different elements are coupled to each other by a *Tie*-constraint.

First, we compute the natural frequencies for all three models and present the results in Tab. 6 One can see that all the natural frequencies coincide ver well. Next we present the *MAC*

	1	2	3	4	5	6
ABAQUS VOLUME f/Hz	14.68	23.65	35.65	39.10	43.33	58.23
ABAQUS SHELL f/Hz	14.51	23.46	34.81	38.41	43.05	57.18
FE2 f/Hz	14.62	23.57	35.50	38.96	43.16	58.00

Table 4. Natural frequencies of the plate

in between the results of ABAQUS VOLUME and FE2 in Fig. 5, which shows the similarity of the results. Finally, we use the upper patch as an actuator with an applied voltage $V_{top} = -1\text{V}$. The

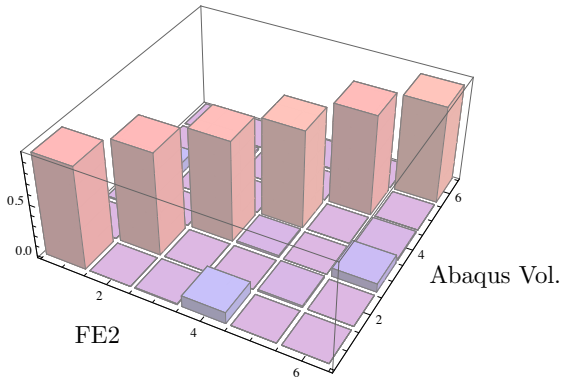

Figure 5. MAC for the rectangular plate with piezoelectric patches

static sensor voltage V_{bot}, the mid point deflection w and the accumalted charge at the actuator Σ_{top} are compared in Tab. 5. Here, we see that the results computed using shell elements in ABAQUS are very far off the ones computed with FE2, but also the ones computed using 3D elements in ABAQUS. In contrast, the results of FE2 and 3D elements in ABAQUS coincide well. From these results we conclude that the coupling of structural shell elements with 3D

	w/m	V_{bot}/V	Σ_{top}/C
ABAQUS SHELL	-4.55×10^{-7}	2.85×10^{-2}	-9.54×10^{-7}
FE2	-1.50×10^{-6}	-5.43×10^{-2}	1.04×10^{-6}
relative error e/%	228.44	90.53	9.49
ABAQUS VOLUME	-1.49×10^{-6}	-4.91×10^{-2}	1.05×10^{-6}
FE2	-1.50×10^{-6}	-5.43×10^{-2}	1.04×10^{-6}
relative error e/%	-0.46	-10.54	0.06

Table 5. Comparison for the static transducer behavior

piezoelectric elements by means of a *Tie*-constraint in ABAQUS may fail and the results are not reasonable. In contrast, the correspondance between our results and the one computed with 3D elements in ABAQUS is good, such that we can conclude on the accuracy and trustworthiness of our formulation of thin piezoelctric shells as material surfaces with mechanical and electrical degrees of freedom.

3.2 Nonlinear shells

In this subsection we seek to verify the geometrically nonlinear behavior for shells. With respect to a comparison to ABAQUS we only consider an elastic shell, because structural shell elements can be used in ABAQUS; no piezoelectric shells are studied in ABAQUS for the following reasons: (1) No electromechanically coupled shell elements are available. (2) The coupling of structural shell elements with 3D piezoelectric elements does not work sufficiently well, as we have just shown in the prevous section on linear plates. (3) Modelling of shells with 3D elements is computationally quite expansive; in particular in nonlinear problems. Therefore, results for piezoelectric shells are only presented using the theory at hand, which we have shown to be sufficiently accurate.

3.2.1 Global snap through buckling of an elastic shell with a rectangular boundary

As mentioned above, we start with the example of a purely elastic shell. It has a plane rectangular boundary that is clamped on all 4 edges; moreover, the tangential plane of the shell surface in the undeformed configuration coincides with this plane for all points along the edges. A sketch of the shell is shown in Fig. 6. As the geometry of the shell stems from

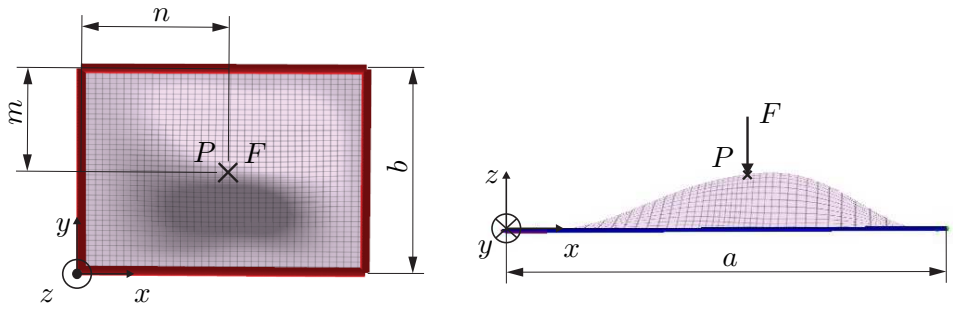

Figure 6. Sketch of the shell

an existing physical structure and has been measured by a geometry scan unit of a Scanning Laser Vibrometer, we do not present any specific data here, other than the dimensions of the boundary rectangle $a \times b = 0.87\text{m} \times 0.62\text{m}$ and the thickness $h = 0.004\text{m}$ of the shell. The material parameters are indentical to the ones used in the plate examples. The shell is modelled with 40×40 elements in FE2 and with 1600 quadratic *S8R5* elements with 8 nodes and 5 degrees of freedom for each node in ABAQUS. A vertical force F is applied in the center point of the plate; Fig. 7 shows the applied force F as a function of the center point displacement. We observe a snap through at a critical force level; this behavior is found with both, FE2 and ABAQUS. ABAQUS *Static* stops the computation at this force value, FE2 reproduces the snap through and proceeds with the computation after the snap through. Here, we were also able to compute the center point deflection for the case of unloading finding a second critical value, at which snap back occurs. In order to reproduce this result the *Riks* method available in ABAQUS was used. In this latter case the deformation is controlled by the center point

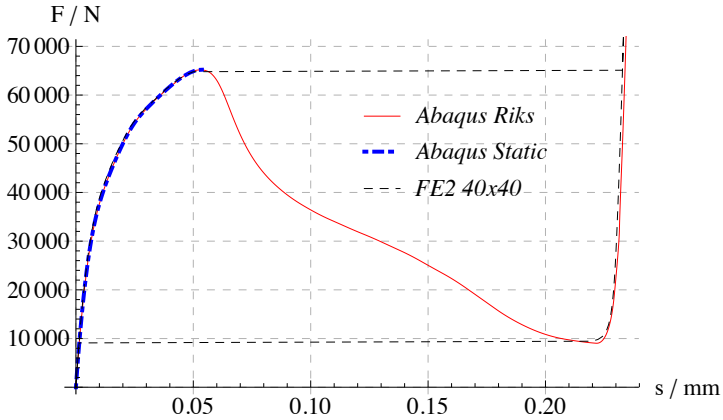

Figure 7. Force - center point displacement curve

displacement. Hence, the instable path can be computed in ABAQUS *Riks*. This method is not implemented in FE2; yet, the critical values obtained by FE2 and by ABAQUS *Riks* are very close and the stable equilibrium paths coincide very well. We conclude on the accuracy of FE2 for geometrically nonlinear elastic problems. As already mentioned we do not present a comparison with ABAQUS for piezoelastic problems, because of the lack of corresponding shell elements in ABAQUS. Nonetheless, from all the results (both, for linear piezoelastic plates and nonlinear elastic shells) we conclude on the general applicability of FE2 to analyse and simulate linear and nonlinear thin piezoelastic shells. The latter case is studied in the next section.

3.2.2 Local buckling of a cylindrical piezoelectric shell

As a second example we study a cylindrical shell with three attached piezoelectric patches, which is clamped at one side. The deformed configuration for a static loading, which acts in the vertical direction and which can be considered as the weight of the shell, is shown in Fig. 8. One can see that a local buckling occurs in the vicinity of the clamping (indicated as a thick blue line in the figure) at the upper side. In order to get a better understanding of the behavior

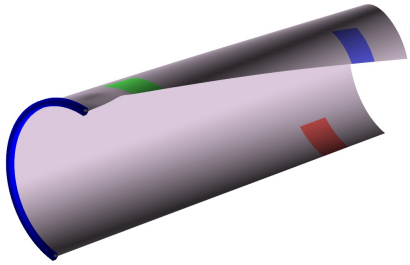

Figure 8. Local buckling of a cylindrical shell with three piezoelectric patches - deformed configuration

of the shell in the geometrically nonlinear regime, the vertical displacements are shown in the left graph of Fig. 9 as a function of the load factor g. The blue curve is the response for the

upper corner point and the red curve for the lower corner point at the free end of the shell. The corresponding results for the voltage measured at the three patches, which are operated in an open-circuit mode, are shown in the right graph. The colors refer to the colors used for the patches in Fig. 9. One can clearly see that once the load factor reaches a critical value (slightly smaller than $g = 6$) the reponse becomes nonlinear. To quantify the critical value we apply

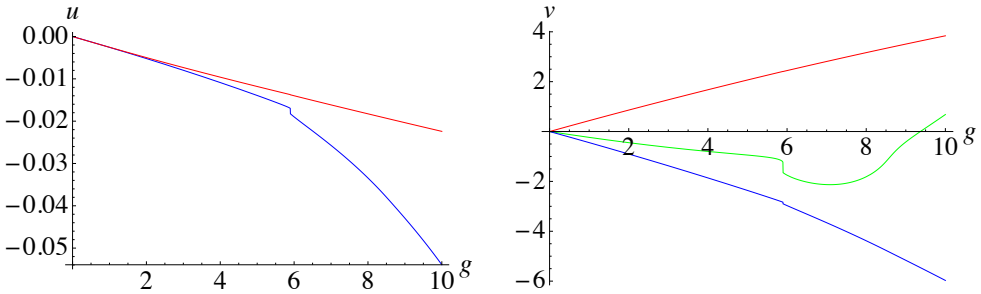

Figure 9. Local buckling of a cylindrical shell with three piezoelectric patches - results: Vertical displacement of corner points (left) and voltage measured at the three patches (right)

the method of an accompanying eigenfrequency analysis for the small amplitude vibrations of the statically pre-deformed shell. The results for the first four eigenfrequencies are shown in Fig. 10; the left graph shows the whole range of variation of the load factor, and the right graph a detailed view on the vicinity of the critical value. From the results shown in the right figure,

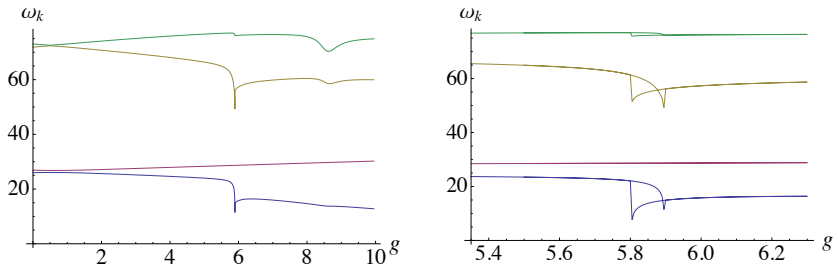

Figure 10. Local buckling of a cylindrical shell with three piezoelectric patches - results: Accompanying eigenfrequency analysis

we see that the critical value, for which the eigenfrequencies become zero, is different for the loading and the unloading case; hence, a snap-through and a snap-back buckling occurs in this problem.

4. Passive shunt damping

For the remainder of the paper we study passive shunt damping using RL-networks for the linear vibrations of plates and shells. Two examples are used. (1) A thin plate to introduce the method of shunt damping in some detail and (2) an existing physical shell, for which the method is experimentally tested.

4.1 An introductary plate example

Here, we use the three layer cantilvered plate from one of the previous examples. The bottom layer is only used as a sensor in an open-circuit to measure the voltage. The upper layer is connected to an electrical network, which consists of a series connection of a resistor R and an inductance L. In case the resistance is zero the electrical network consisting of a parallel circuit of the capacity C_p of the piezoelectric layer or patch and the inductance L is

$$\omega_e = \frac{1}{\sqrt{LC_p}}. \tag{32}$$

In order to compute an optimal value for R and L we use a method introduced by Ahmadian [9] and Hagood and von Flotow [10]. The result for the optimal values to damp the vibrations in the vicinity of the n-th natural frequency is

$$L_{opt} = \frac{1}{\omega_e^2 \tilde{C}_p} \quad \text{and} \quad R_{opt} = \frac{r_{opt}}{\omega_n^{sc} \tilde{C}_p}, \tag{33}$$

with

$$\tilde{C}_p = C_p(1 - k_{31,n}^2)\ , \quad \omega_e = \omega_n^{oc}\sqrt{1 + k_{31,n}^2} \quad \text{and} \quad r_{opt} = \sqrt{2}\frac{k_{31,n}}{1 + k_{31,n}^2}. \tag{34}$$

Here, the effective electromechanical coupling cooeficient (EMCC) for the n-th natural frequency is computed as

$$k_{31,n}^2 = \frac{(\omega_n^{oc})^2 - (\omega_n^{sc})^2}{(\omega_n^{sc})^2}, \tag{35}$$

where ω_n^{sc} is the n-th natural frquency for short-circuit conditions and ω_n^{oc} the one for open-circuit conditions.

In Fig. 11 results for the cantilevered plate are presented, for which the target frequency is the first natural frequency. In the upper left plot the optimal value for the resitor is used with different values for the inductance, whereas in the upper right plot the optimal value for the inductance is used together with different values for the resistor. On can see the very good damping characteristics for using both optimal values. The lower two plots present the voltage measured at the bottom piezoelectric layer, which is only used as a sensor in open-circuit conditions. Concerning the experimental verification of passive shunt damping of thin plates we refer to Berger et.al. [11].

4.2 Experimental validation on a real shell

In this subsection the method of passive shunt damping is used to damp the vibrations a thin shell; simulation results as well as experimental results are presented. The shell is shown in Fig. 12. The geometry of the elastic substrate shell is identical to the one used in 3.2.1. Two patches are attached; one at the top and one at the bottom. The location and the dimensions of the piezoelectric patches are the same as in 3.1.2. Concerning the boundary conditions, the

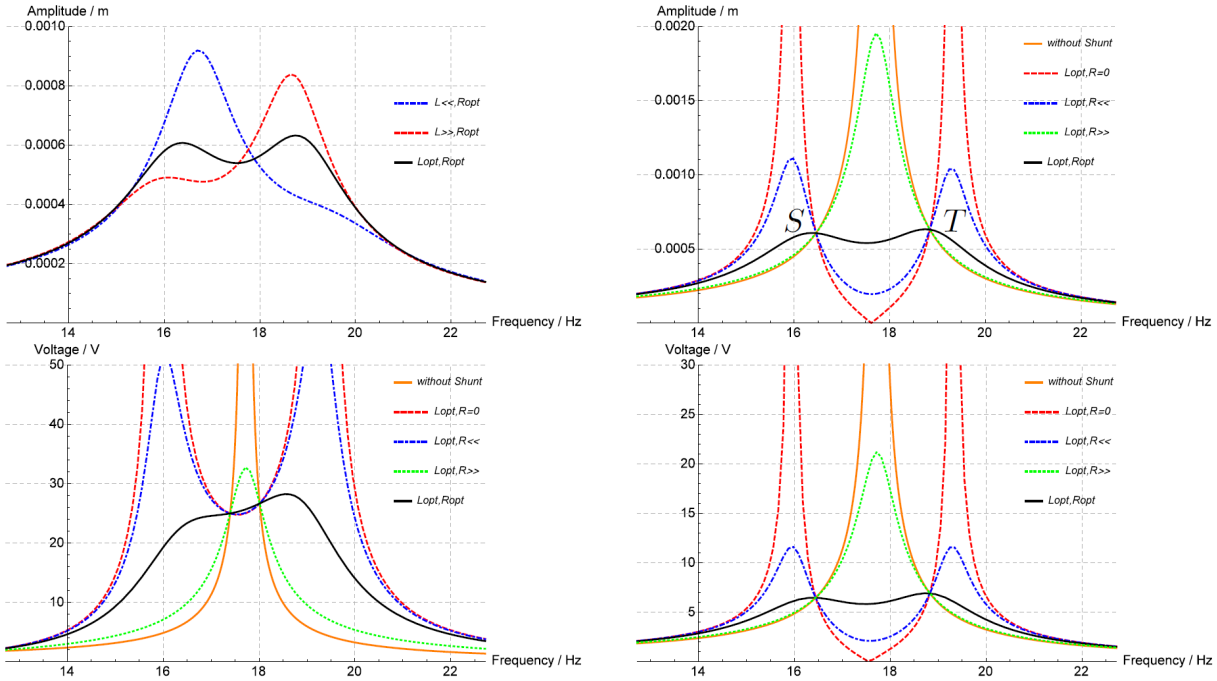

Figure 11. Dynamic magnification factor for cantilvered plate with Shunt damping

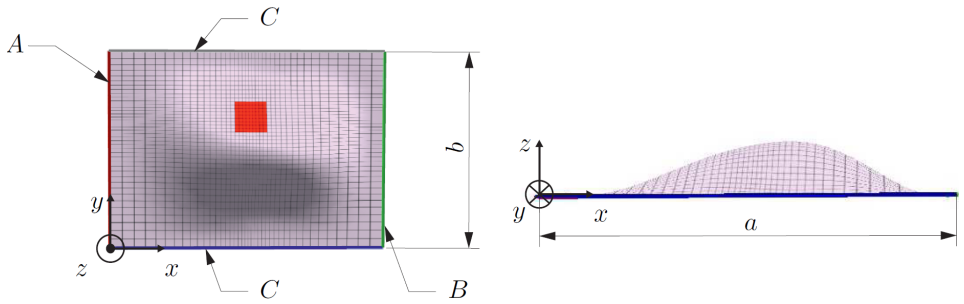

Figure 12. Sketch of the shell with piezoelectric patches

two sides denoted as C are clamped, the side denoted as B is simply supported with in-plane displacement and the side denoted as A is simply supported with a free displacement in the x-direction. The natural frequencies are given in Tab. 6. The RL-network is connected to the patch

Natural frequency	1	2	3	4	5	6
FE2 f/Hz	62.11	87.37	102.43	180.47	202.67	247.56

Table 6. Natural frequencies of the shell

at the upper side and the patch at the lower side is used as a sensor in an open-circuit; hence, the voltage can be measured. The optimal values for the resistor and the inductance are computed

to damp the vibrations in the vicinity of the fifth natural frequency. Te dynamic magnification for the case no shunt is connected is shown in the left plot in Fig. 13 in the range of the fourth, fifth and sixth natural frequency. The right plot shows the behavior in the vicinity of the fifth natural frequency with the connected RL-network. The optimal value for the inductance is used in all curve, but the resistor vaue R is varied. One can see the good damping characteristics in the case the optimal values for both, resistor and inductance, are used. Finally, we discuss

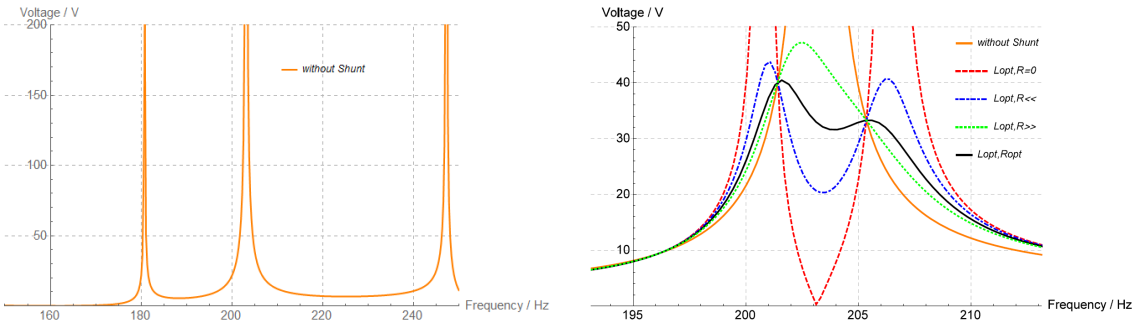

Figure 13. Dynamic magnification factor the shell without and with shunt damping

some experimental results for passive shunt damping of the shell we have used in this example. The experimental setup is shown in Fig. 14. The dimensions of the shell and the piezoelectric patches as well as the location of the patches are the ones we have just used in the simulation. Two types of practical realizations of the RL-network are used. In one case the RL-network

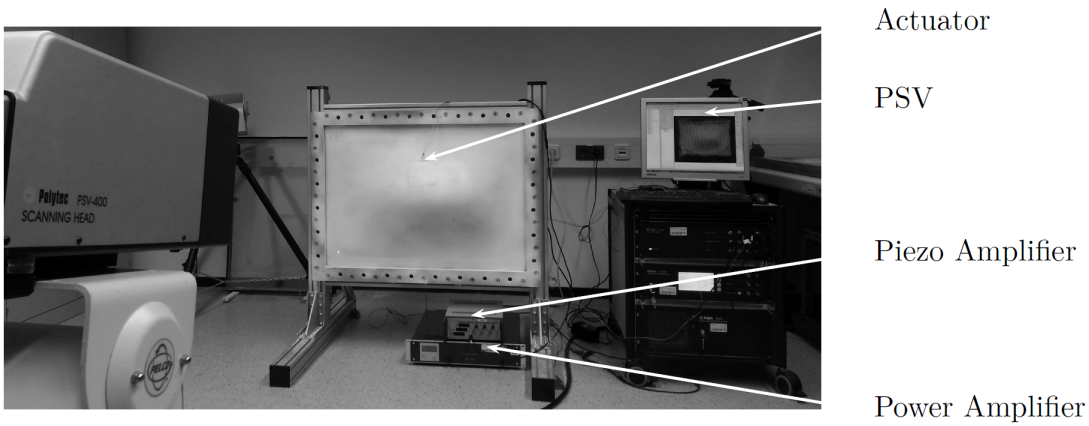

Figure 14. Experimental setup

is put into practice by means of a Gyrator and in the other case by means of an RL-decade. For these two cases the values for the RL-network are given in Tab. 7. The computed ones are the optimal values based on a measurement of the capacity of the piezoelectric patch and the target frequency, which is the fifth natural frequency. The other ones have been obtained from the experiments; it is worth noting that the ones using the RL-decade are very close to the computed ones, but the resistor value R for the Gyrator case is much higher than the computed

one, because of the high input resistance of the Gyrator, which does not allow to use the optimal value. In the experiment the shell is excited by an electrodynamic shaker and the amplitude of

	computed	Gyrator	RL-decade
R	1.48H	1.56H	1.48H
L	81.64Ω	375Ω	77.9Ω

Table 7. Values for R and L used in the experiment

the center point deflection is measured with a Laser Scanning Vibrometer. The results with and without passive shunt damping are shown in Fig. 15. The thick black curves correspond to the values in Tab. 7. From the results we conclude that passive shunt damping works reasonably well and the vibrations in the vicinity of the target frequency are significantly reduced.

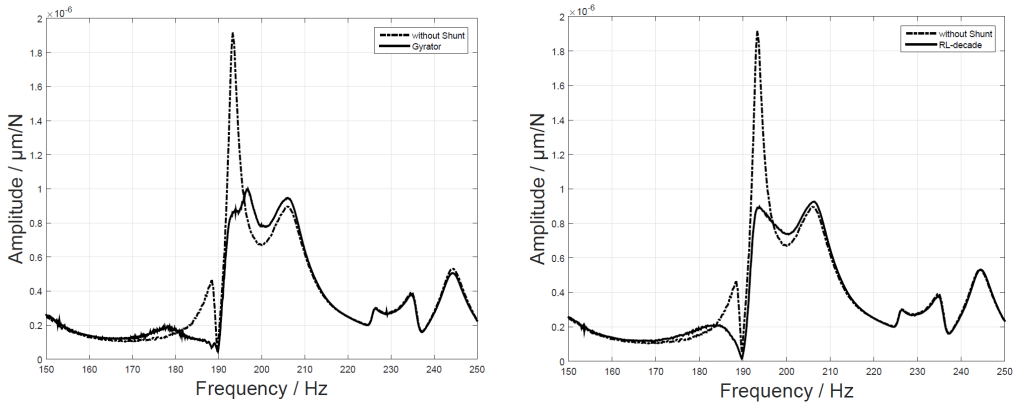

Figure 15. Experimental results for passive shunt damping: Gyrator (left) and RL-decade (right)

5. CONCLUSIONS

In the present paper we have introduced an efficient formulation for thin shells with piezoelectric transducers in the geometrically nonlinear regime, which considers the shell as a material surface with mechanical and electrical degrees of freedom. Results computed with this theory have been compared to numerical solutions computed with commerciqally available Finite Elements; in particular with ABAQUS using 3D elements in order to account for the electromechanical coupling. A very good agreement was found, with a significantly reduced numerical effort when using the present shell formulation. Finally, passive shunt damping has beeen studied numerically and experimentally showing the practical applicability of passive shunt damping under realistic conditions.

ACKNOWLEDGEMENTS

We acknowledge the support of this work from the Linz Center of Mechatronics GmbH in the framework of the COMET-K2 programme. We would also like to thank the Fraunhofer LBF and the LOEWE Zentrum AdRIA in Darmstadt for their support of the experimental work.

References

[1] M. Krommer, The Significance of Non-Local Constitutive Relations for Composite Thin Plates Including Piezoelastic Layers with Prescribed Electric Charge. *Smart Materials and Structures*. **12**(3), 318–330, 2003.

[2] R.C. Batra, S. Vidoli, Higher Order Piezoelectric Plate Theory Derived from a Three Dimensional Variational Principle. *AIAA Journal*, **40**, 91–104, 2002.

[3] E. Carrera, M. Boscolo, Classical and mixed finite elements for static and dynamic analysis of piezoelectric plates. *International Journal for Numerical Methods in Engineering*, **70**(10), 1135–1181, 2007.

[4] Y. Vetyukov, A. Kuzin, M. Krommer, Asymptotic splitting in the three-dimensional problem of elasticity for non-homogeneous piezoelectric plates. *International Journal of Solids and Structures*, **48**, 12–23, 2011.

[5] E. Carrera, S. Brischetto, P. Nali, *Plates and Shells for Smart Structures: Classical and Advanced Theories for Modeling and Analysis*. John Wiley & Sons, Chichester, 2011.

[6] V. Eliseev, Y. Vetyukov, Finite deformation of thin shells in the context of analytical mechanics of material surfaces, *Acta Mechanica*. **209**, 43–57, 2010.

[7] Y. Vetyukov, *Nonlinear Mechanics of Thin-Walled Structures: Asymptotics, Direct Approach and Numerical Analysis*. Springer, Vienna, 2014.

[8] Y. Vetyukov, Finite element modeling of Kirchhoff-Love shells as smooth material surfaces. *ZAMM*, **94**, 150–163, 2014.

[9] N.W. Hagood, A. von Flotow, Damping of structural vibrations with piezoelectric materials and passive electrical networks. *Journal of Sound and Vibration*, **146**(2), 243–268, 1991.

[10] M. Ahmadian, K.M. Jeric, On the application of shunted piezoceramics for increasing accoustic transmission loss in structures. *Journal of Sound and Vibration*, **243**(2), 347–359, 2001.

[11] G. Zenz, W. Berger, J. Gerstmayr, M. Nader, M. Krommer, Design of piezoelectric transducer arrays for passive and active modal control of thin plates. *Smart Structures and Systems*, **12**(5), 547–577, 2013.